Comparison of Cushioning Mechanisms between Cellular Glass and Gabions Subjected to Successive Boulder Impacts

C. W. W. Ng, F.ASCE[1]; Y. Su[2]; C. E. Choi[3]; D. Song[4]; C. Lam[5]; J. S. H. Kwan[6]; R. Chen[7]; and H. Liu[8]

Abstract: Gabions are the most commonly adopted cushion layer for shielding rigid debris-resisting barriers against boulder impact. Despite the prevalent use of gabions, they comprise heavy rock fragments that are not easily transported up steep natural terrain. The advent of using light-weight cellular glass as an alternative cushion layer provides an innovative approach for absorbing impact energy. However, a lack of insight on their load attenuation characteristics has hindered its potential implementation. In this study, cellular glass was subjected to successive impacts to replicate the dynamic loading of boulders by using a large-scale pendulum setup. Results reveal that for a single impact at 70 kJ, crushing exhibited by cellular glass leads to 25% lower impact force compared to gabions, which rely predominantly on rock fragment rearrangement to absorb energy. However, gabions exhibit more effective load spreading, with a diffusion angle three times greater than cellular glass. To ensure robust designs for cellular glass, the Johnson's damage number is proposed to quantify the plastic deformation and to improve estimates of the cushioning efficiency represented by the load-reduction factor (K_c) used in current design. **DOI: 10.1061/(ASCE)GT.1943-5606.0001922.**

Author keywords: Debris flow; Boulder impact; Crushable foam; Large nonlinear finite-element modeling; Johnson's damage number D_n; Load-reduction factor K_c.

Introduction

Debris flows entrain and transport large boulders that are capable of incapacitating structures along their flow path (Cui et al. 2015; Zeng et al. 2015). Clusters of boulders generally accumulate at the front of a torrent via particle-size segregation (Johnson et al. 2012). To shield structures against boulders and to extend their working life, cushion layers are commonly installed in front of barriers (Calvetti and di Prisco 2009; Peila et al. 2007). One of the critical considerations in the design of cushion layers is their ability to attenuate multiple and successive impacts from clusters of boulders commonly found at the front of geophysical flows (Lambert et al. 2014).

Gabions, comprising rock fragments inside steel-wire cages, are the most commonly adopted cushion layer because they are durable and simple to construct. However, gabions are less practical when heavy rock fragments are not easily transported up steep natural terrain (Choi and Cheung 2013), or when the self-weight of the cushioning material is an important design consideration, such as cushioning on top of rockfall protection galleries. Large-scale impact tests have been conducted to study the cushioning performance of gabions (Heymann et al. 2010, 2011; Lambert et al. 2009, 2014). Results show that the large deformation induced by rock fragment rearrangement attenuates loading under high impact energy. Ng et al. (2016) carried out large-scale pendulum tests to study the performance of confined gabion cushions at energy levels of up to 70 kJ for up to six successive impacts. Results reveal that the high crushing strength of the rock fragments inhibits further dissipation of energy after the irreversible rearrangement of rock fragments diminishes under successive impacts. The implication is that impact and transmitted forces for gabions can only increase without an additional mechanism for energy dissipation aside from rock fragment rearrangement. Certainly, a more efficient cushion layer at attenuating successive impacts is warranted.

[1]Chair Professor, Dept. of Civil and Environmental Engineering, Hong Kong Univ. of Science and Technology, Clear Water Bay, Kowloon 999077, Hong Kong.

[2]Geotechnical Engineer, Dept. of Civil and Environmental Engineering, Hong Kong Univ. of Science and Technology, Clear Water Bay, Kowloon 999077, Hong Kong; JSTI Group, No. 8 East Fuchunjiang Rd., Jianye District, Nanjing 210017, China.

[3]Research Assistant Professor, Dept. of Civil and Environmental Engineering, The HKUST Jockey Club Institute for Advanced Study, Hong Kong Univ. of Science and Technology, Clear Water Bay, Kowloon 999077, Hong Kong (corresponding author). Email: ceclarence@ust.hk

[4]Associate Professor, Key Laboratory of Mountain Hazards and Earth Surface Process/Institute of Mountain Hazards and Environment, Institute of Mountain Hazards and Environment, Chinese Academy of Sciences, #.9, Block 4, Renminnanlu Rd., Chengdu 610041, China.

[5]Geotechnical Engineer, Geotechnical Engineering Office, Civil Engineering and Development Department, the Government of the Hong Kong Special Administrative Region, 101 Princess Margaret Rd., Kowloon 999077, Hong Kong.

[6]Chief Geotechnical Engineer, Geotechnical Engineering Office, Civil Engineering and Development Department, the Government of the Hong Kong Special Administrative Region, 101 Princess Margaret Rd., Kowloon 999077, Hong Kong.

[7]Associate Professor, Dept. of Civil and Environmental Engineering, The Harbin Institute of Technology, HIT Campus of Univ. Town of Shenzhen, Shenzhen 518055, China.

[8]Research Student, Dept. of Civil and Environmental Engineering, Hong Kong Univ. of Science and Technology, Clear Water Bay, Kowloon 999077, Hong Kong.

Note. This manuscript was submitted on March 21, 2017; approved on February 21, 2018; published online on June 25, 2018. Discussion period open until November 25, 2018; separate discussions must be submitted for individual papers. This paper is part of the ***Journal of Geotechnical and Geoenvironmental Engineering***, © ASCE, ISSN 1090-0241.

The search for a more lightweight cushion layer that is also capable of reducing transmitted loads under successive impacts has led to great interest in crushable materials. Recently, cellular glass has been explored as a cushion system for rock fall protection galleries (Schellenberg et al. 2007). Cellular glass is produced by baking recycled glass fines with mineral additives. Cellular glass has the advantages of being lightweight, nonflammable, water resistant, and ecofriendly. However, limited tests have been carried out to study the dynamic loading behavior of cellular glass. Schellenberg et al. (2006) carried out large-scale drop tests simulating impact energies of up to 15 kJ. Results revealed that the maximum boulder impact force, F_{max}, with cellular glass are 10% smaller, compared with sand and gravel. Despite the useful insight obtained from their study, current understanding can be further enhanced by simulating higher impact energies and by investigating the deformation and load transmission characteristics of cellular glass. This will enable engineers to adopt this new material to better protect barriers and galleries in mountainous regions around the world.

In this study, the fundamental dynamic response of cellular glass under successive impact is investigated using a large-scale pendulum impact setup. The physical test results are then used to calibrate a nonlinear finite-element model. The calibrated numerical model is subsequently adopted to carry out numerical back-analyses to bear further insight on the cushion mechanisms of crushable glass under successive impacts.

Gibson and Ashby Model

In this study, the Gibson and Ashby model was adopted to model the compressive stress-strain behavior of cellular glass (Gibson and Ashby 1997). A single cube of cellular glass with nominal dimensions of 50 mm was subjected to compression following the ASTM D1621 (ASTM 2010) to obtain the mechanical behavior of cellular glass. The measured compressive stress-strain behavior is shown in Fig. 1. For comparison, an idealized stress-strain curve based on the Gibson and Ashby model is shown. The theoretical compressive stress-strain behavior based on the Gibson and Ashby model comprises three key loading stages, specifically elastic, plateau, and densification. In the first stage, the loading is characterized as linear elastic deformation of the closed-cell walls. The deformation of the closed-cell wall exhibits a linear elastic response under crushing strains (<15%) and can be characterized as follows:

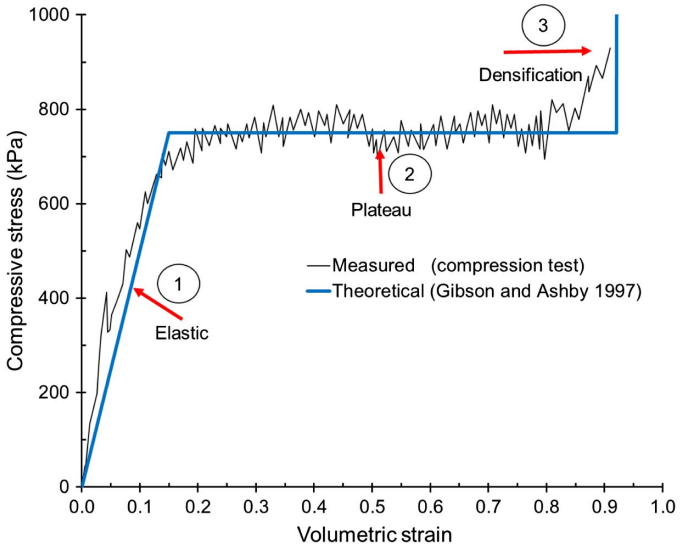

Fig. 1. Measured and idealized compressive stress-strain curves of cellular glass.

$$\sigma = E \times \varepsilon = \left[\varphi^2\left(\frac{\rho^*}{\rho_s}\right)^2 + (1-\varphi)\frac{\rho^*}{\rho_s}\right] E_s \times \varepsilon (\sigma \le \sigma_c) \quad (1)$$

where σ = compressive stress (MPa); E = measured foam elastic modulus (5 MPa); E_s = solid modulus (MPa); ε = volumetric strain; σ_c = foam crushing strength (0.75 MPa); ρ^* = measured foam density (140 kg/m^3); ρ_s = solid density (2,500 kg/m^3); φ = fraction of solid contained in the cell edges (0.8); and $1-\varphi$ = fraction of solid contained in the cell faces (0.2).

The second stage of loading is a plateau associated with crushing of the closed-cell walls and can be described as follows:

$$\sigma = \sigma_c = \left[0.2\left(\varphi\frac{\rho^*}{\rho_s}\right)^{3/2} + (1-\varphi)\left(\frac{\rho^*}{\rho_s}\right)\right]\sigma_{fs}(\varepsilon_c < \varepsilon < \varepsilon_D) \quad (2)$$

where ε_c = crushing strain; ε_D = limiting strain; and σ_{fs} = solid fracture strength (kPa).

At higher compressive strains, the closed-cell walls have completely collapsed and opposing cell walls come in contact with each other. Further loading is solely taken by the material of the cell walls themselves. As the cell walls are loaded, the stiffness is equivalent to an elastic modulus E_s up to a limiting strain

$$\varepsilon_D = 1 - 1.4\left(\frac{\rho^*}{\rho_s}\right) = 1 - 1.4R_e \quad (3)$$

where ρ^* = measured foam density (140 kg/m^3); ρ_s = solid density (2,500 kg/m^3); and R_e = relative density (0.06). When R is substituted into Eq. (3), the calculated limiting strain ε_D is 0.92.

Hertz Impact Equation

The elastic impact force can be estimated using the Hertz equation (Hungr et al. 1984). This elastic solution assumes an impact between a sphere and a plane based on Hertz contact theory (Johnson 1985)

$$F = \frac{4E}{3}R^{\frac{1}{2}}(\delta)^{\frac{3}{2}} \quad (4)$$

where F = boulder impact force; E = effective modulus of elasticity; R = boulder radius; and δ = elastic boulder penetration depth. The effective modulus is given as $1/E = (1-\nu_1^2)/E_1 + (1-\nu_2^2)/E_2$ where E_1 and E_2 are the elastic moduli of barrier and concrete boulder, respectively; and ν_1 and ν_2 are the Poisson's ratios of the barrier and concrete boulder, respectively, to account of energy loss due to plastic deformation.

To simplify Eq. (4) for the design of rigid reinforced concrete barriers, Kwan (2012) proposed a simplified equation, which is given as follows:

$$F = K_c 4000 v^{1.2} R^2 \quad (5)$$

where v = impact velocity; R = boulder radius; and K_c = empirical load-reduction factor. This equation is based on typical values of elastic parameters for a spherical concrete boulder and a rigid reinforced concrete barrier. The value of the load-reduction factor is recommended as 0.1 (Hungr et al. 1984) for the scenario where a granite boulder impacts a rigid reinforced concrete barrier.

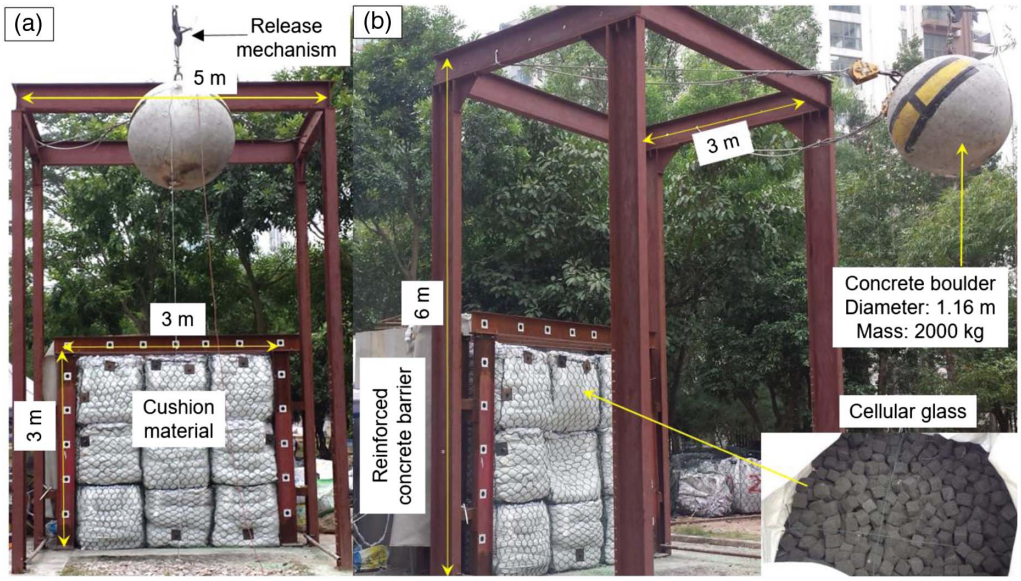

Fig. 2. Impact test setup: (a) front view; and (b) oblique view.

Experimental Field Tests

Pendulum Impact Test Setup

The test setup comprises a rigid barrier, a cushion layer, and a steel frame to suspend and swing a concrete boulder. The rigid barrier is 3 m in height, 3 m in width, and 1.5 m in thickness [Figs. 2(a and b)]. The steel frame is used to suspend a 2,000-kg concrete ball that has a 1.16-m diameter. The steel frame occupies a plan area of 5×3 m, and has a height of 6 m. The 1-m thick cellular glass cushion layer was installed in front of the rigid barrier and confined using a steel frame around its peripheral to reduce lateral displacement during impact.

Instrumentation

A uniaxial accelerometer (maximum range 200 g) was installed on the concrete boulder to measure its acceleration during the impact process. The measured boulder impact force is the product of acceleration and boulder mass. Eight load cells (maximum range 220 kN) were installed on the rigid barrier to measure the horizontal and vertical transmitted load distributions. The load cell surface used in this study was 150 mm in length and 150 mm in width. The location of each load cell is shown in Fig. 3. The impact process was captured using two video cameras. One is a high-speed camera capable of capturing 200 frames per second (fps) at a resolution of 672×672 pixels was installed on one side of the test setup. Another camera capable of capturing images at up to 30 fps was installed at the opposite side of the test setup. The data logger captures data at 10 kHz. After each impact, the surface deformation was surveyed using a laser displacement sensor.

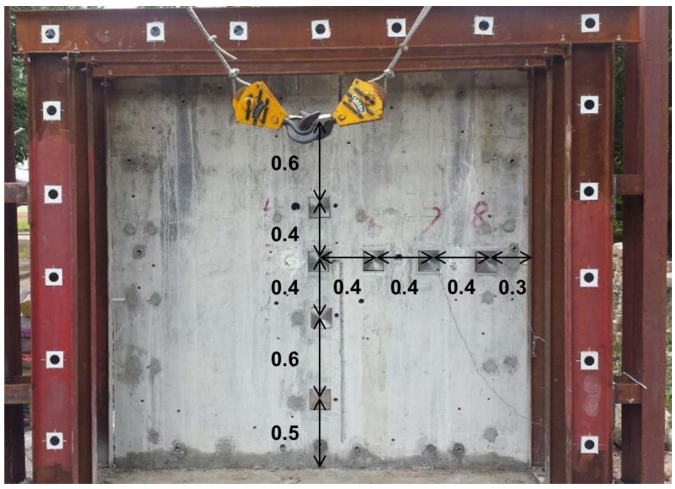

Fig. 3. Front view of rigid barrier and load-cell layout (in meters).

Properties of Cellular Glass and Gabion

Cellular glass comprises 50 mm cubes with a density of 140 kg/m^3. The measured crushing strength of the cubes was about 0.75 MPa. The cellular glass cubes were placed in bulk bags and then in nine separate gabion baskets. The bulk density of the filled gabions was about 110 kg/m^3. The bulk bags were stacked together to form a $3 \times 3 \times 1$ m cushion layer. They were anchored to the rigid barrier using steel bolts and tied to the reinforced concrete wall around its perimeter.

A typical gabion cell comprises of rock-filled baskets tied together using 3 mm diameter steel wires (Ng et al. 2016). The entire gabion cushion layer comprised nine cubical gabion cells with a nominal length of 1 m. The unit weight of each gabion cell was about 1,500 kg/m^3. The size of the granitic fragments used to fill gabions ranged from 160 to 300 mm.

Test Program

After installation of the cellular glass cushion layer, the concrete ball was suspended using a crane truck to a target height of 1 and 3.5 m to induce impact energies of 20 and 70 kJ, respectively. The concrete boulder was then released from the crane and allowed to impact the cushion layer. After each impact, the surface deformation was surveyed. Successive impacts were carried out accordingly.

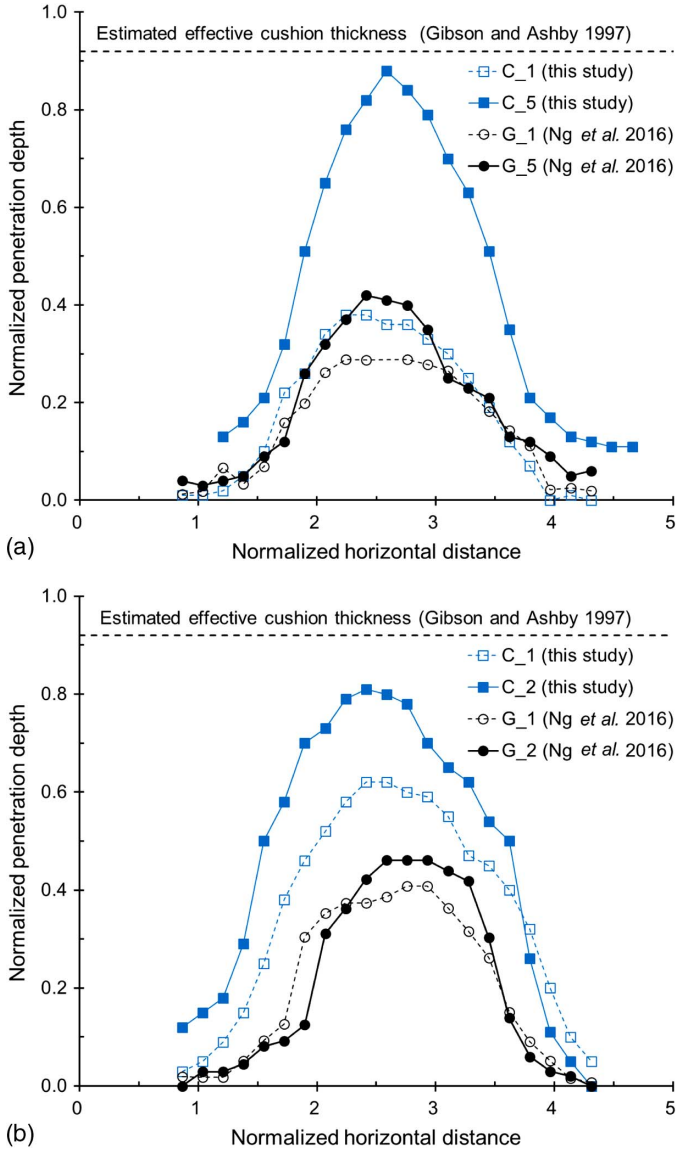

Fig. 4. Measured penetration depths under successive impacts: (a) 20 kJ; and (b) 70 kJ.

Field Test Results and Analyses

Measured Penetration Depths

The penetration depth is one of the most critical design considerations for assessing the required thickness of the cushion layer. The normalized measured penetration profiles for cellular glass and gabion under successive impacts are compared at energy levels of 20 kJ [Fig. 4(a)] and 70 kJ [Fig. 4(b)]. In the test identification numbers, C and G represent cellular glass and gabions, respectively. The deformation profiles are shown with the normalized horizontal distance from the center of the 3-m wide barrier. The measured penetration depth is normalized by the 1-m thick cushion layer. The horizontal length of the gabion cushion layer is normalized by the boulder radius (0.58 m) to provide a clear indication of the load-spreading capability of each cushion layer. As discussed previously, during the densification stage for the cellular glass, the limiting strain (ε_D) was reached and cell wall crushing no longer contributes to the ability of cellular glass to attenuate loading. Based on the limiting strain, the effective cushion thickness is estimated as follows:

$$\delta_e = e \times \varepsilon_D = e \times (1 - 1.4R_e) \tag{6}$$

where δ_e = estimated effective cushion thickness; e = cushion layer thickness (1 m); and R_e = relative density (0.06). The calculated effective cushion thickness is 0.92 m. It is assumed that the cushion layer is a continuous cellular glass sheet. The difference between adopting a continuous sheet and cubes of cellular glass will be discussed later. For cellular glass, the measured maximum penetrations are all smaller than the estimated effective cushion thickness for successive impacts at both 20 and 70 kJ. This means that the cushioning mechanism of crushing is evidently effective at attenuating boulder impact loads for successive impacts.

The first impact at 20 kJ induces a normalized maximum penetration depth of 0.4, equivalent to 40% of the initial thickness of the cushion layer [Fig. 4(a)]. By contrast, the maximum penetration depth of gabion after the first impact is about 30% of the original thickness of the cushion layer. The difference in the maximum penetration depth is attributed to the different mechanical responses exhibited by the cellular glass and gabion. Cellular glass is a crushable material with a crushing strength of 0.75 MPa, whereas the unconfined compressive strength of the granite rock fragments in the gabion cell is in the order of 120 MPa (Alvarez Grima and Babuška 1999). The low crushing strength of cellular glass enables large deformation as the closed-cell walls collapse. In contrast, gabions rely on the irreversible rearrangement of rock fragments to dissipate energy, which provides less deformation.

Similarly, at an impact energy of 70 kJ [Fig. 4(b)], the maximum penetration depth increases as expected. Under a higher impact energy, cellular glass reaches 80% penetration of its initial thickness only after the second impact. To prevent damage to instrumentation, no further successive impacts were carried out. A comparison of the deformed profiles for the cellular glass and gabion after the first impact at 70 kJ is shown in Figs. 5(a and b), respectively. The close-up views show that cellular glass crushes and deforms locally. By contrast, less crushing is observed for gabions, therefore the deformation profile is less localized and more load spreading is observed. Cubes of cellular glass were used in this study rather than a continuous sheet. The cubes initially undergo rearrangement with each other. Once the glass cubes reach a dense enough configuration, crushing takes over as the dominant mechanism of energy dissipation. The two distinct cushion mechanisms of crushing and rearrangement serve important ramifications for the measured boulder impact force and transmitted load distributions, which will be discussed later.

Attenuation of Boulder Impact Force under Successive Impacts

Mechanical Response under Successive Impacts at 20 kJ

Aside from deformation characteristics, a robust cushion layer design must be able to attenuate the boulder impact force. A comparison of the boulder impact force between cellular glass and gabion at an impact energy level of 20 kJ is shown in Figs. 6(a and b). The boulder impact force is the product of the measured acceleration and mass of the concrete boulder. The deduced penetration depth is obtained by carrying out successive integration of the measured acceleration of the boulder. The estimated elastic relationships between the boulder impact force and penetration depth for cellular glass and gabion at 20 kJ using the Hertz equation [Eq. (4)] are shown for reference. In the Hertz equation, a measured elastic modulus of 5 MPa was adopted for cellular glass and an elastic modulus of 16 MPa (Bourrier et al. 2011) was adopted for gabion.

For cellular glass, the measured F_{max} of 93 kN resulted in a maximum penetration depth of 0.55 m after the first impact.

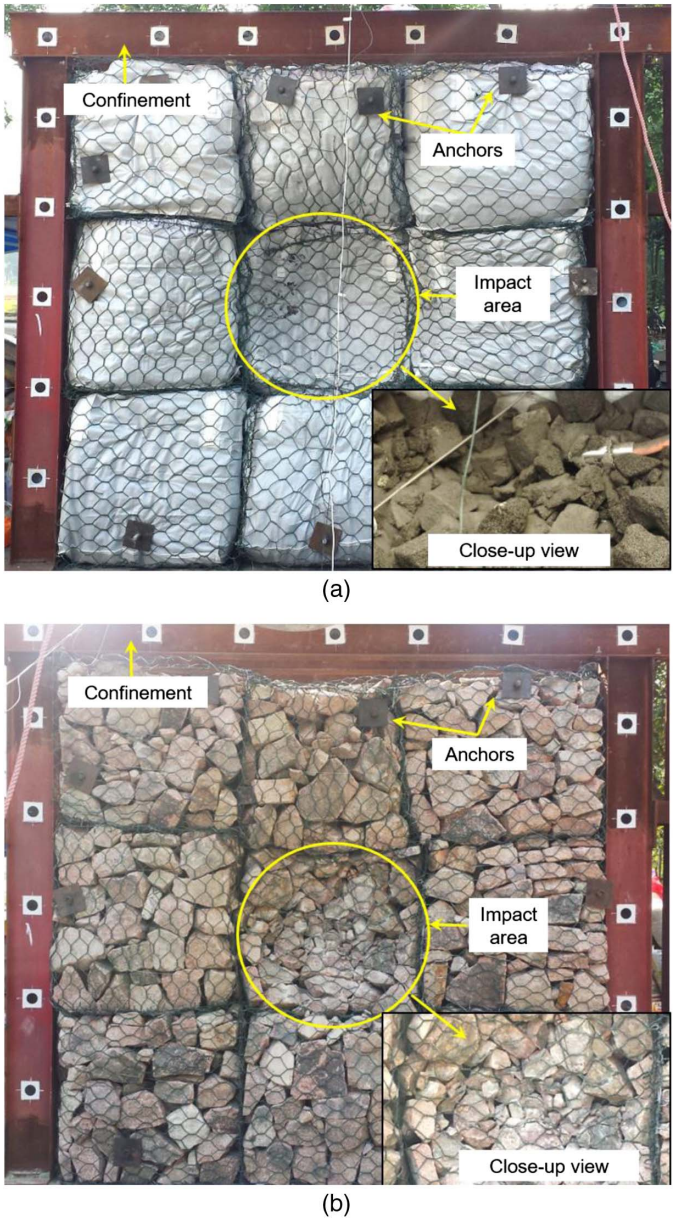

Fig. 5. Front view of deformed profile after first impact: (a) cellular glass; and (b) gabion.

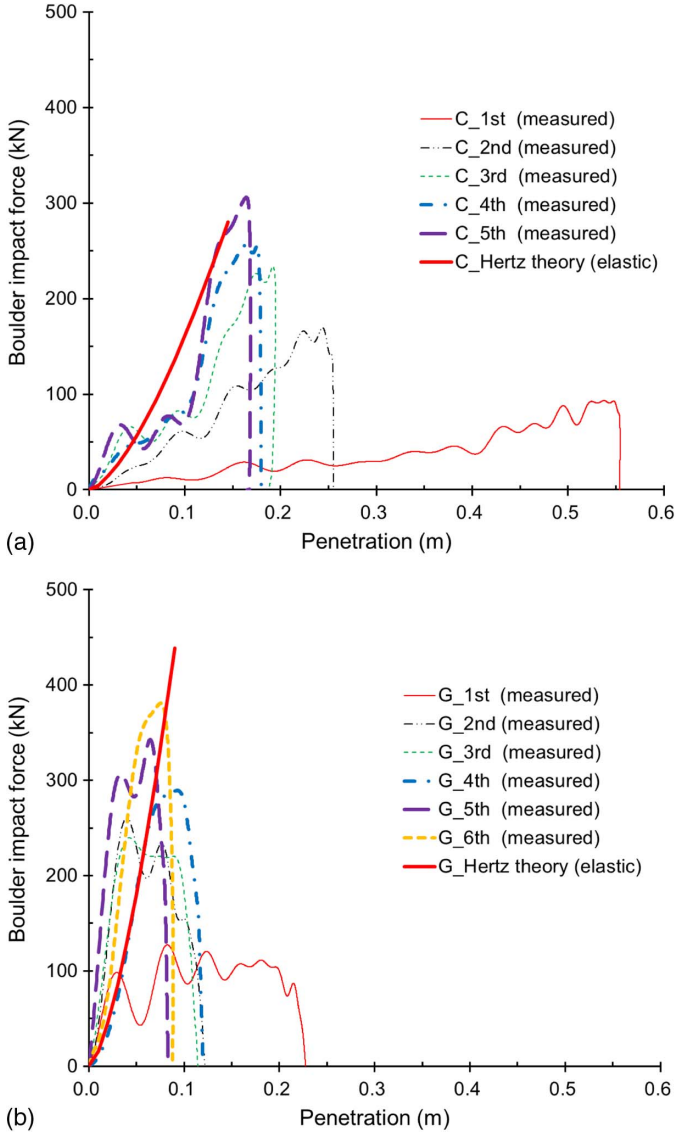

Fig. 6. Comparisons of measured responses between (a) cellular glass; and (b) gabion at 20 kJ.

The maximum penetration deduced by double integration of the boulder acceleration is much larger than measured maximum penetration of 0.3 m. This is due to the settlement of the cushion layer under gravity after each impact. After the impact force reaches its maximum, the unloading stiffness, represented by the slope of measured curve for cellular glass, is much steeper than loading modulus. This implies that plastic deformation dominates the deformation of the cushion layer, resulting in a significant amount of energy being absorbed. By carrying out successive integration of the boulder force with respective to the penetration distance, the calculated energy is 20 kJ, meaning all the impact energy is absorbed by cellular glass. This agrees with the numerical simulations carried out by Bourrier et al. (2011), demonstrating that an increase in the ratio between the unloading and loading modulus leads to higher plastic strains, and thus more energy dissipation. By adopting an elastic modulus of 5 MPa, the F_{max} deduced from cellular glass using the Hertz equation [Eq. (4)] is 280 kN and the maximum penetration depth is estimated as 0.15 m. The Hertz equation leads to an overestimate of the F_{max} by up to three times. Evidently, an elastic assumption is conservative when cellular glass crushes to prolong the impact duration to reduce the impact force. Furthermore, plastic deformation induced by the rearrangement of cellular glass cubes reduces the impact force further compared to a continuous cellular glass sheet.

A comparison of cellular glass between successive impacts at 20 kJ show that the F_{max} increases with successive impacts. The F_{max} for fifth impact is about three times larger compared to the first impact. This is attributed to the reduced maximum penetration [Fig. 6(a)] due to the reduced cushion layer thickness, which decreases with successive impacts. The maximum penetration for the first impact is 3.4 times larger compared to the fifth impact. Less plastic deformation increases the F_{max} with successive impacts. This indicates that the cushion efficiency of cellular glass decreases with successive impacts. By contrast, the calculated absorbed energies for successive impacts are all about 20 kJ. It means that the cellular glass maintains constant and predictable energy absorption for all successive impacts.

An impact energy of 20 kJ on the gabion cushion layer resulted in a measured F_{max} of 127 kN and a maximum penetration depth of

0.23 m deduced using successive integration of the measured boulder acceleration (Ng et al. 2016). The deduced maximum penetration of 0.23 m is slightly smaller than the measured maximum penetration depth of 0.3 m. The difference is caused by the irregular shape of the rock fragments as the deformed profile was surveyed. In Fig. 6(b), the curves of gabion for the first impact are more fluctuating compared to cellular glass. The observed fluctuations during the impact process is caused by the collapse of force chains and formation of new ones through particle rearrangement (Lambert et al. 2009). Force chains transmitting high forces may become unstable if the surrounding fragments do not provide sufficient confining stress (Bertrand et al. 2005). Particle rearrangements may induce large plastic deformation and force chain collapse may further contribute to the dissipation of impact energy. The calculated absorbed energy was 20 kJ for gabion during the first impact. The F_{max} predicted by the elastic Hertz solution is higher by about 3.4 times compared to measured impact force, implying that rock fragment rearrangements play an important role in its cushion mechanism.

As expected, similar to cellular glass, the F_{max} of gabion increases with successive impacts. This is because of the progressive densification of the gabion cushion layer, permitting less plastic deformation through irreversible rock fragment rearrangement with successive impacts. Successive impacts also lead to closer rock fragments contacts that strengthen force chains. This can explain why the loading curve for the sixth impact is much smoother compared to that of the first impact. The calculated absorbed energies are all 20 kJ for successive impacts, further corroborating that gabion cushion layers provide stable and predictable energy absorption under successive impacts.

Mechanical Response under Successive Impacts at 70 kJ

Figs. 7(a and b) show the boulder impact forces between cellular glass and gabion at an impact energy level of 70 kJ, respectively. The measured F_{max} for the first impact is 2.8 times and 3.3 times smaller compared to the estimated F_{max} using Eq. (4). This demonstrates that both cellular glass and gabion can provide cushion performance under high impact energies. Also, the F_{max} for the second and sixth impacts are 1.8 and 2.2 times larger compared with the first impact for cellular glass and gabion, respectively. Note that for cellular glass, the time to maximum boulder impact force or penetration is the same for successive impacts. However, for gabion, the boulder impact force reaches its maximum load before its maximum penetration. This is attributed to the cellular glass being dominated by a crushing mechanism, which induces less plastic deformation during unloading. For gabion, the collapse of force chains generates new force chains, which in turn induce fragment rearrangements during the unloading process.

Comparisons of Mechanical Responses between Cellular Glass and Gabion

The cushion performances of cellular glass and gabion, specifically the F_{max} [Fig. 8(a)] and the load-reduction factor K_c [Fig. 8(b)], are compared for successive impacts. A comparison between the measured F_{max} demonstrates that the impact force for cellular glass is up to 17 and 25% smaller compared to gabion for the first impact at the energy levels of 20 and 70 kJ, respectively. Furthermore, the F_{max} of cellular glass are all smaller than gabion for the successive impacts at both energy levels of 20 and 70 kJ. This means that the cellular glass can provide better cushion performance by reducing the boulder impact force compared to gabion for successive impacts. This is because of larger plastic deformation induced by crushing enables smaller F_{max} compared to irreversible rock fragment rearrangement.

Fig. 8(b) shows the deduced load-reduction factor (K_c) for each successive impact at the energy levels of 20 and 70 kJ. For both cellular glass and gabion, K_c values increase with successive

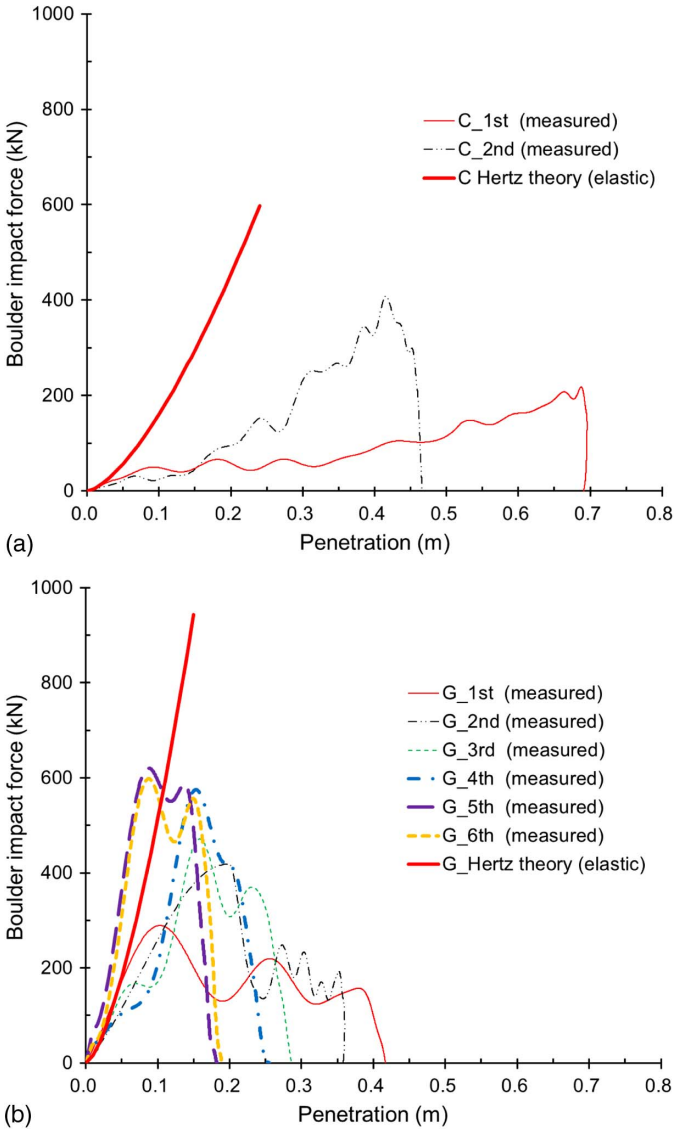

Fig. 7. Comparisons of measured responses between (a) cellular glass; and (b) gabion at 70 kJ.

impacts, implying that cushion efficiency decreases with the number of successive impacts. Note that the K_c value of gabion at 20 kJ are 30% larger compared to 70 kJ for sixth impact. This means the gabion performs better at 70 kJ compared to an impact energy of 20 kJ under successive loading. This can be explained by the fact that plastic deformation decreases rapidly for successive impacts at impact energy of 20 kJ. The maximum deduced penetration is 0.23 m for the first impact in Fig. 6(b). For successive impacts, the penetrations decreases to 0.1 m. It means that the plastic deformation decreases quickly and the cushion efficiency decreases rapidly under successive impacts. By contrast, the deduced maximum penetrations [Fig. 7(b)] at the energy level of 70 kJ decrease progressively for successive impacts. This indicates that gabions have better cushion efficiency up to 30% at 70 kJ compared to 20 kJ under successive impacts.

Distribution of Transmitted Loads on the Rigid Barrier

Time Histories of Transmitted Loads for the First Impact

The time histories of the transmitted load for the first impact on cellular glass at 70 kJ are shown in Fig. 10(a). Four load cells were

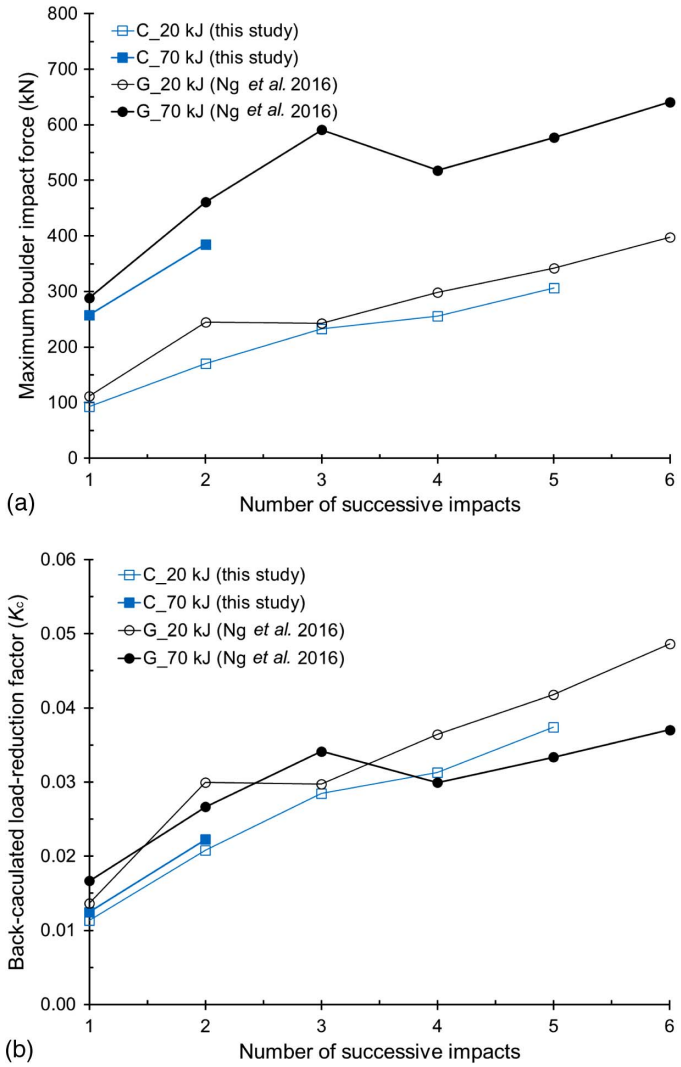

Fig. 8. Performances of cushion layers under successive impact: (a) maximum ball impact force; and (b) back-calculated load-reduction factor (K_c).

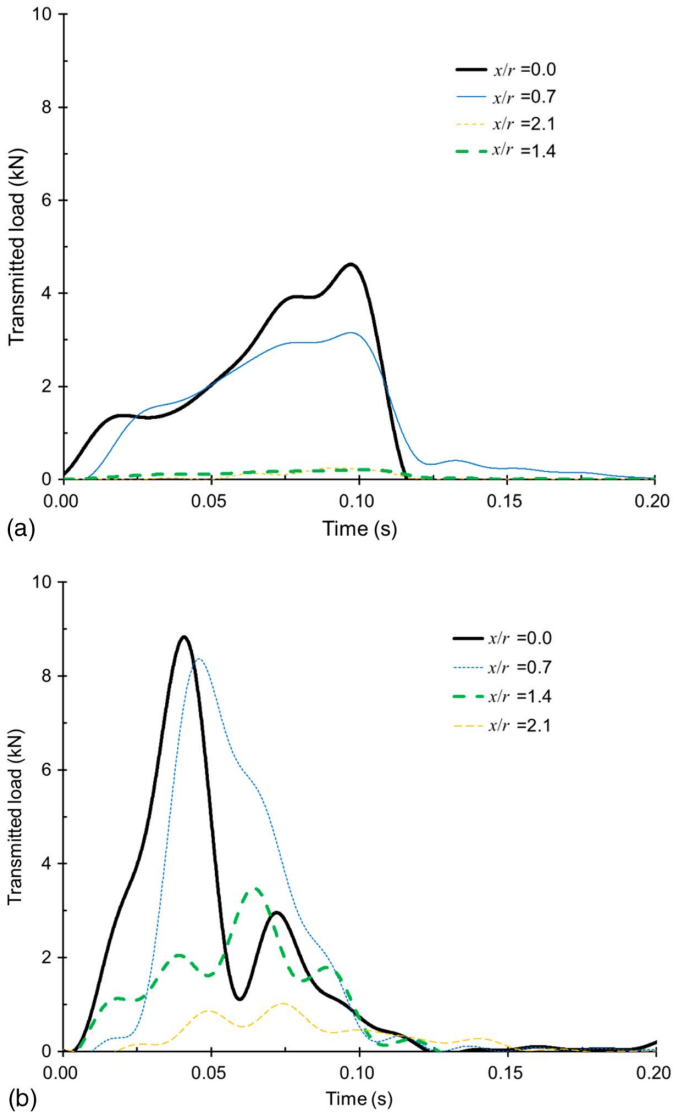

Fig. 10. Transmitted load time histories with varying normalized horizontal distances for 70 kJ: (a) cellular glass; and (b) gabions.

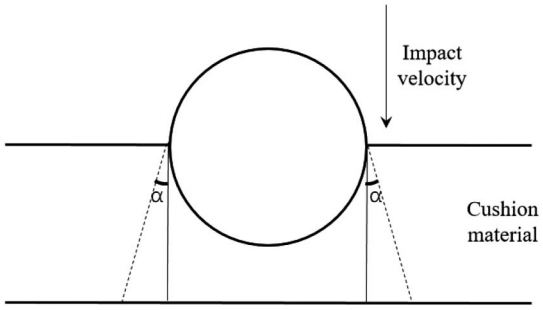

Fig. 9. Load diffusion schematic diagram.

installed along the horizontal centerline of the barrier in Fig. 3. The horizontal distance from the center of the barrier (x) is normalized by the boulder radius (r). The impact point of boulder is directly at the center of the barrier. The maximum transmitted loads are 4.6 and 3.2 kN at the normalized horizontal distances of 0.0 and 0.7, respectively. Maximum transmitted loads of only 0.2 kN were measured at a normalized distance of distance of 1.4 and 2.1. Results imply that the load mostly concentrated near the center of rigid barrier. A precise load diffusion angle cannot be established due to a lack of measurements between normalized distance of 0.7 and 1.4. However, if it is assumed that the maximum load diffusion extent is at a normalized distance of 1.4, the load diffusion angle of cellular glass is estimated as 12° for the first impact (Fig. 9). The estimated load diffusion angle is relatively small and this demonstrates that crushing limits the ability of a cushion to spread load. By contrast, a high transmitted load of 1.3 kN is measured at a normalized distance of 2.1 for gabion [Fig. 10(b)]. Results shows that load transmission is more efficient for gabion compared to cellular glass. The mechanism of load transmission in gabion depends on the stability of force chains of the rock fragments (Muthuswamy and Tordesillas 2006). The stability of force chains depend on the number of particles, meaning that force chains with a larger number of particles will have a greater likelihood of potential failure (Anthony and Marone 2005; Zhang et al. 2017). Furthermore, the high crushing resistance and the large rolling resistance of large rock fragments used in gabion cushion layers increase the stability of the force chains and thus transmission (Muthuswamy and Tordesillas 2006). Measured results indicate that the load diffusion angle for gabion is 32°, which is about three times larger than

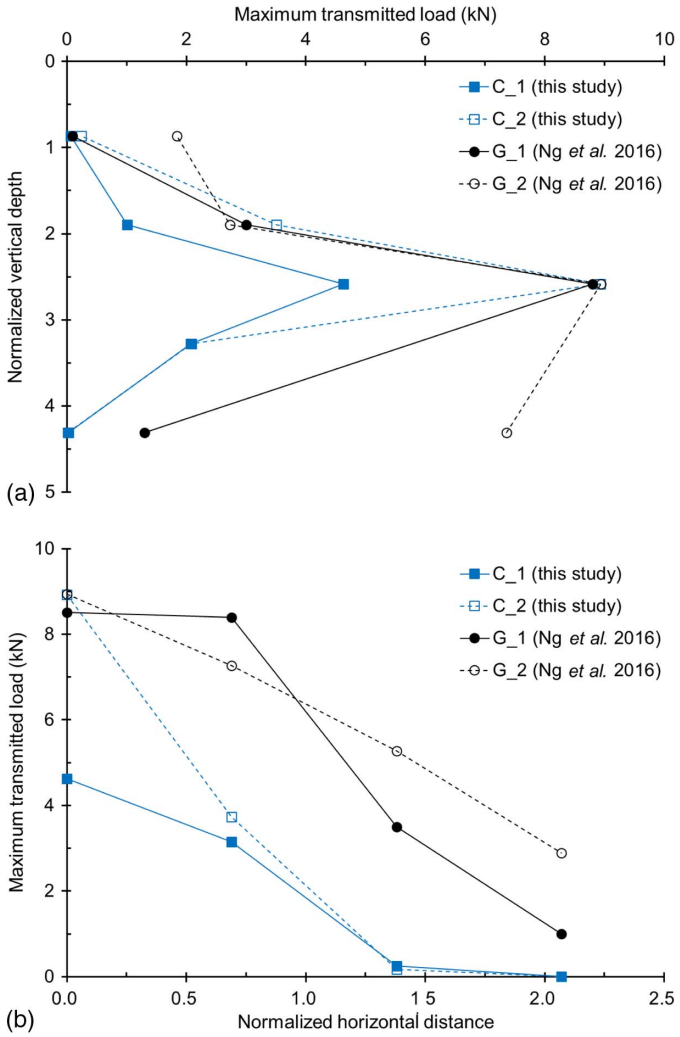

Fig. 11. Transmitted load distributions on the rigid barrier at 70 kJ: (a) vertical; and (b) horizontal.

cellular glass. It is apparent that load transmission through fragment rearrangement is more effective at load diffusion the load compared to localized crushing in cellular glass.

Load Distributions under Successive Impacts

The vertical [Fig. 11(a)] and horizontal [Fig. 11(b)] load transmission distributions are compared for cellular glass and gabion at an energy level of 70 kJ. To prevent damage to instrumentation, only two successive impacts were carried out on cellular glass for 70 kJ. The first and second impacts for both cushion materials are compared. The vertical and horizontal distances of each load cell are normalized by boulder radius. For cellular glass [Fig. 11(a)], no load was registered at the uppermost load cell five for the first impact. By contrast, at an equal distance downward from the center of the barrier, a maximum transmitted load of 1.3 kN was measured. This shows that loads are more readily transmitted downward, attributing to higher confining stress at the bottom of the cushion layer. Similar effects were also observed for gabion cushion layers in Ng et al. (2016). The maximum transmitted load at a normalized vertical distance of 2.6 for second impact is twice as large as the first impact. This is because a larger boulder impact force is measured for the first impact. Furthermore, the reduced cushion layer thickness increases load transmission to the center of rigid barrier. A comparison between cellular glass and gabion

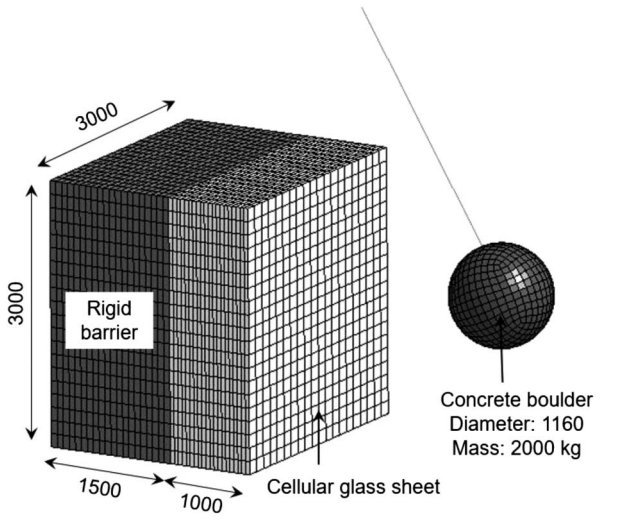

Fig. 12. Three-dimensional numerical model setup (in millimeters).

demonstrates that the maximum transmitted load at a normalized vertical distance of 2.5 is about twice as large for the gabion cushion layer. Again, this corresponds to the larger boulder impact forces induced on the gabion cushion layer compared to the cellular glass cushion layer. Also loads are more readily transmitted through force chains that have high crushing strength. However, only a slight difference between the maximum transmitted loads during the first and second impacts are measured for gabion. This can be caused by uneven contacts between gabion and load cell on the rigid barrier.

Similarly, the load distribution for the first impact of cellular glass along the horizontal plane [Fig. 10(b)] shows that that no load is generated at normalized distances of 1.4 and 2.1. Results reveal that that the load diffusion angle of cellular glass does not change significantly under successive impacts. By contrast, at the same horizontal distances, much larger transmitted loads are observed for the gabion cushion. The slope of transmitted load distribution of gabion for the first impact is much steeper than the second successive impact. This shows that the load is more uniformly distributed on the rigid barrier with a densified gabion cushion layer. Also, the load diffusion effect for gabion increases under successive impacts. Results show that cellular glass can provide more substantial load reduction compared to gabion cushion layers. Cellular glass shows promising potential for field application.

Numerical Modeling for Cellular Glass

In this study, the finite-element method was adopted to investigate the effects of crushing strength of cellular glass on cushion efficiency at various impact energies. The software package LS-DYNA (2012) for analyzing large deformation and the dynamic response of structures was used. Details of the numerical model setup and modeling procedures are discussed as follows.

Numerical Model Setup

The numerical setup adopts the same geometric configuration as that of the physical tests (Fig. 12). The total number of nodes and solid elements equal 16,136 and 9,350, respectively. The only difference is that a continuous sheet of cellular glass is simulated for simplicity rather than the cubes used in the physical tests. It will be demonstrated later that that the rearrangement of cellular glass cubes only influence the initial stages of the first impact.

Table 1. Model parameters

Property	Value
Foam density (kg/m^3)	140
Crushing strain	0.15
Limiting strain	0.92
Crushing strength (MPa)	0.75
Solid fracture strength (MPa)	57.27
Poisson's ratio	0.05
Elastic modulus (MPa)	5
Solid modulus (MPa)	380
Tensile stress cut-off (MPa)	0.1
Damping coefficient	0.5

The mechanism of crushing dominates the mechanical response of cellular glass thereafter. Furthermore, the same impact energy (70 kJ) and orientation from the experiments are applied using a model ball. In the numerical model, the concrete boulder is modeled using shell elements and the cellular glass is modeled using solid elements. The cellular glass is modeled by the material Type 63 "MAT_CRUSHABLE_FOAM" (LS-DYNA 2012). This material model required the input of five parameters: material density, elastic modulus, Poisson's ratio, stress strain curve, tensile stress cutoff, and damping coefficient. The first four parameters were from the laboratory test results. Tensile cutoff and viscous damping coefficient were obtained from the literature review. This material model enables the implementation of stress-strain behavior to simulate the crushing behavior of cellular glass. During implementation, the Young's modulus is assumed to be a constant and is used to update the stress values assuming elastic behavior before the crushing strength is reached. Cellular glass under compression can be assumed to deform one-dimensionally with a Poisson's ratio of 0.05 (Jackson 2010). A foam density of 140 kg/m^3, crushing strain of 0.15, crushing strength of 0.75 MPa, and elastic modulus of 5 MPa are measured from compression test in the laboratory. The limiting strain and solid modulus are computed based on the Gibson and Ashby model. Experimental testing, such as resonant column tests, is useful in elucidating the damping properties of cellular glass at small strain and will enable an improved prediction of its dynamic behavior. However, capturing the damping properties of cellular glass that undergoes large strains due to crushing may impose challenges that merit further investigation. A summary of the parameters used in the model is given in Table 1.

Influence of Adopting Cellular Glass Cubes and a Continuous Sheet

The boulder impact force and penetration time histories at an energy level of 70 kJ in the field tests were used to calibrate the numerical model. Figs. 13(a and b) show comparisons of boulder impact force and penetration depth between measured and computed results. Results show that the computed boulder impact force is larger compared to the physical tests. By contrast, the penetration depth is smaller in the numerical simulations compared to the physical tests. The differences are because of the rearrangement of cellular glass cubes that extends the impact duration, thus reducing the F_{max}. It is found that the difference of F_{max} between measured and computed results is about 20%, indicating that crushing still dominants the cushion mechanism of cellular glass.

Parametric Study of Crushing Strength

A series of numerical simulations were carried out to study the effects of crushing strength on the cushion performance of the

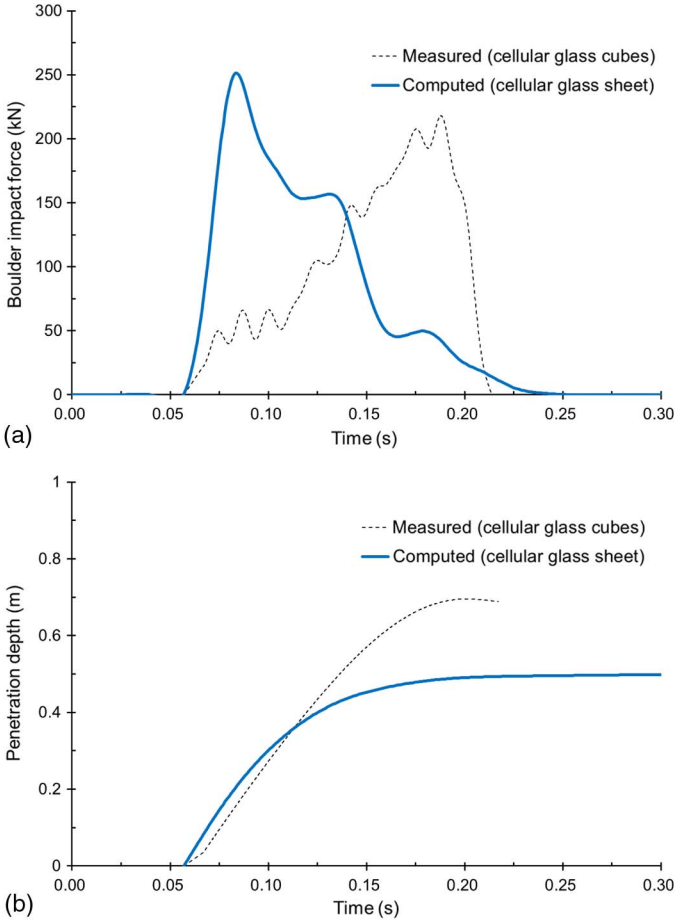

Fig. 13. Measured and computed results of 1-m thick cellular glass cushion layer at 70 kJ: (a) boulder impact force; and (b) penetration.

cellular glass at various impact energies. Measured results show that larger plastic deformation induces better cushion performances during impact. Johnson (1972) proposed an approach for assessing the extent of plastic deformation of metals subjected to impact loading using a dimensionless number defined as follows (Zhao 1998):

$$D^n = \rho v^2/\sigma_0 \tag{7}$$

where ρ = material density (kg/m^3); σ_0 = material compressive stress (Pa); and v = impact velocity (m/s). By assuming no impact energy is lost before the boulder impacts on the cushion layer, the impact velocity is determined from Eq. (8)

$$v = \sqrt{\frac{2I}{m}} \tag{8}$$

where I = impact energy (kJ); and m = boulder mass (kg). The damage number (D^n) can be used to represent the induced plastic strain during loading. In this study, the Johnson's damage number is proposed to quantify the plastic deformation and to improve estimates of the cushion efficiency represented by back-calculated load-reduction factors (K_c).

Fig. 14 shows the relationship between the back-calculated load-reduction factor K_c and Johnson's damage number D^n for different crushing strengths and impact velocities. Solid lines represent the computed results by adopting four typical crushing resistances ranging from 0.25 to 1.00 MPa (Zegowitz 2010). Based on the Gibson and Ashby model, four estimated foam densities were back-calculated by using Eq. (2) and summarized in Table 2.

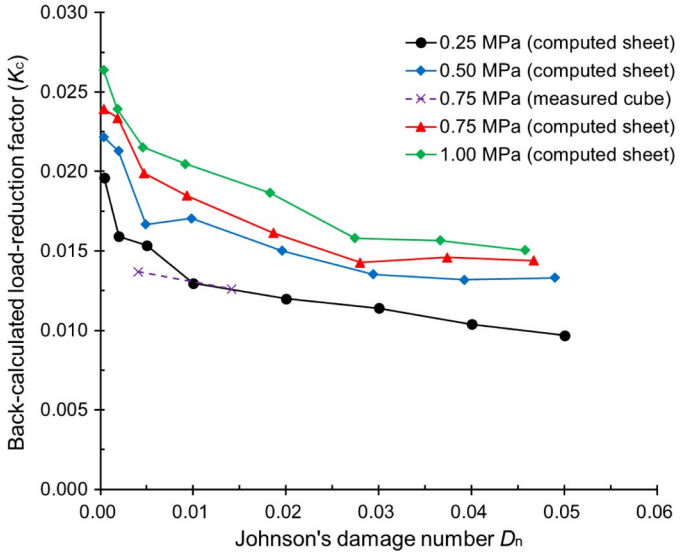

Fig. 14. Back-calculated load-reduction factor K_c and Johnson's damage number D^n of cellular glass of various crushing strengths.

Table 2. Summary of parameters used in parametric study

Foam density (kg/m^3)	Elastic modulus (MPa)	Crushing strength (MPa)	Crushing strain	Limiting strain	Impact energy (kJ)
50	1.6	0.25	0.155	0.97	2, 10, 25, 50, 100,
98	3.3	0.50	0.151	0.95	150, 200, 250
140	5.0	0.75	0.150	0.92	
183	6.8	1.00	0.147	0.90	

It is found that the crushing strain is observed to decrease with both density and crushing strength. For each crushing strength, eight different impact energies were simulated. The elastic modulus E was determined by Eq. (1) and summarized in Table 2. It is shown that E increases with the foam density and crushing strength. Based on Eq. (7), it is clear that D^n increases with impact energy for the same crushing strength. Results show that the K_c of cellular glass decreases with D^n induced by increasing impact energy. This means that cellular glass has better cushion efficiency with increasing impact energy. This is caused by the higher impact energies that lead to larger plastic deformation, meaning that cushion efficiency increases with impact velocity. Note that to find that the slope of each curve decreases with impact velocity. This is because at low impact energy the mechanical response of cellular glass is primarily dominated by an elastic response (Fig. 1). Plastic deformation induced by increasing impact energy leads to increasing cushion efficiency and a rapidly diminishing K_c. At high impact energies, the plastic deformation dominates the mechanical response. The cushion efficiency increases with the plastic deformation and K_c decreases slower compared to low impact energy. It implies that the cellular glass has better cushion performances at higher impact energy.

Johnson's damage number also decreases with crushing strength under the same impact energy. Comparisons between each crushing strength shows that load-reduction factors decrease with the Johnson's damage number induced by decreasing crushing strengths. This implies that higher crushing strength reduces cushioning efficiency. This is because of the large crushing strength that inhibits the plastic deformation of cellular glass during impact and increasing boulder impact force. However, larger plastic deformation induced by lower crushing strength may also decreases the cushion efficiency under successive impacts. Furthermore, practitioners may consider using the damage number to better predict the cushion efficiency of cellular glass with the consideration of different crushing strengths.

Moreover, due to the rearrangement of cellular glass cubes initially during loading, the measured load-reduction factor is smaller than the computed results. A smaller load-reduction factor means that the F_{max} is lower with better cushion performance. Results indirectly suggest that cellular glass cushioning layers installed as cubes will provide better cushion effect compared to a continuous cellular glass sheet. It may be more practicable to transport cubes of cellular glass up steep mountainous terrain rather than a bulky continuous sheet.

Conclusions

A series of large-scale pendulum impact tests were conducted and numerical back-analyses were carried out using the finite-element method to understand the fundamental deformation characteristics and cushioning mechanism of cellular glass. Results for the energy levels tested in this study reveal the following:

- The cushion mechanism of crushing exhibited by cellular glass is more effective at attenuating boulder impact forces and reducing transmitted loads to the barrier under successive impacts compared to gabions. Cellular glass provides up to 25% and 50% reduction of maximum boulder impact forces and transmitted loads to the barrier, respectively, compared to the conventional use of gabion at 70 kJ for a single impact.
- Gabions are more effective at spreading the impact load laterally compared to cellular glass, which deforms locally under successive impact. Gabions rely on the irreversible rearrangement of rock fragments to more effectively diffuse loads under successive impacts compared to cellular glass. The diffusion angle for gabion is at least three times greater compared to that of cellular glass for the first impact.
- Results demonstrate that the cushioning efficiency represented by the back-calculated load-reduction factor (K_c) decreases with crushing strength of cellular glass and its corresponding impact energy. Practitioners may use the damage number to better predict the cushion efficiency of cellular glass with consideration of different crushing strengths.
- It is revealed from finite-element analyses that the cushioning performance of cellular glass could be more efficient at attenuating impact compared to a continuous cellular glass sheet. Cellular glass cubes rearrange during the initial loading process, thus further enhancing load attenuation.

Acknowledgments

This paper is published with the permission of the Head of the Geotechnical Engineering Office, and the Director of Civil Engineering and Development of the Government of the Hong Kong Special Administrative Region. The authors are grateful for financial support from the theme-based research grant T22-603/15-N provided by the Research Grants Council of the Government of Hong Kong Special Administrative Region, China. The authors would like to gratefully acknowledge the support of the HKUST Jockey Club Institute for Advanced Study and the Chinese Academy of Sciences (CAS) Pioneer Hundred Talents Program.

References

Alvarez Grima, M., and R. Babuska. 1999. "Fuzzy model for the prediction of unconfined compressive strength of rock samples." *Int. J. Rock Mech. Min. Sci.* 36 (3): 339–349. https://doi.org/10.1016/S0148-9062(99)00007-8.

Anthony, J. L., and C. Marone. 2005. "Influence of particle characteristics on granular friction." *J. Geophys. Res.* 110 (B8): 1–14. https://doi.org/10.1029/2004JB003399.

ASTM. 2010. *Standard test method for compressive properties of rigid cellular plastics*. ASTM D1621. West Conshohocken, PA: ASTM.

Bertrand, D., F. Nicot, P. Gotteland, and S. Lambert. 2005. "Modelling a geo-composite cell using discrete analysis." *Comput. Geotech.* 32 (8): 564–577. https://doi.org/10.1016/j.compgeo.2005.11.004.

Bourrier, F., S. Lambert, A. Heymann, P. Gotteland, and F. Nicot. 2011. "How multi-scale approaches can benefit the design of cellular rockfall protection structures." *Can. Geotech. J.* 48 (12): 1803–1816. https://doi.org/10.1139/t11-072.

Calvetti, F., and C. di Prisco. 2009. "An uncoupled approach for the design of rockfall protection tunnels." *Struct. Eng. Int.* 19 (3): 342–347. https://doi.org/10.2749/101686609788957892.

Choi, K. Y., and R. W. M. Cheung. 2013. "Landslide disaster prevention and mitigation through works in Hong Kong." *J. Rock Mech. Geotech. Eng.* 5 (5): 354–365. https://doi.org/10.1016/j.jrmge.2013.07.007.

Cui, P., C. Zeng, and Y. Lei. 2015. "Experimental analysis on the impact force of viscous debris flow." *Earth Surf. Process. Landforms* 40 (12): 1644–1655. https://doi.org/10.1002/esp.3744.

Gibson, L. J., and Ashby, M. F. 1997. *Cellular solids—Structures and properties*. 2nd ed. Cambridge, UK: Cambridge University Press.

Heymann, A., M. Collombet, S. Lambert, and P. Gotteland. 2011. "Use of external testing methods to assess damage on rockfall protection structures." *Appl. Mech. Mater.* 82: 704–709. https://doi.org/10.4028/www.scientific.net/AMM.82.704.

Heymann, A., S. Lambert, E. Haza-Rozier, G. Vinceslas, and P. Gotteland. 2010. "An experimental comparison of half-scale rockfall protection sandwich structures." In *Proc., Structures under Shock and Impact XI -SUSI XI*. Southampton, UK: Wit Press.

Hungr, O., G. C. Morgan, and R. Kellerhals. 1984. "Quantitative analysis of debris torrent hazards for design of remedial measures." *Can. Geotech. J.* 21 (4): 663–677. https://doi.org/10.1139/t84-073.

Jackson, K. E. 2010. "Predicting the dynamic crushing response of a composite honeycomb energy absorber using solid-element-based models in LS-DYNA." In *Proc., 11th Int. LS-DYNA Users Conf.*. Livermore, CA: Livermore Software Technology Corporation.

Johnson, C. G., B. P. Kokelaar, R. M. Iverson, M. Logan, R. G. LaHusen, and J. M. N. T. Gray. 2012. "Grain-size segregation and levee formation in geophysical mass flows." *J. Geophys. Res.* 117 (F1): F01032. https://doi.org/10.1029/2011JF002185.

Johnson, K. L. 1985. *Contact mechanics*. London, UK: Cambridge University Press.

Johnson, W. 1972. *Impact strength of materials*. London: Edward Arnold.

Kwan, J. S. H. 2012. *Supplementary technical guidance on design of rigid debris-resisting barriers*. GEO Rep. No. 270. Hong Kong: Geotechnical Engineering Office.

Lambert, S., P. Gotteland, and F. Nicot. 2009. "Experimental study of the impact response of geocells as components of rockfall protection embankments." *Nat. Hazard. Earth Syst. Sci.* 9 (2): 459–467. https://doi.org/10.5194/nhess-9-459-2009.

Lambert, S., A. Heymann, P. Gotteland, and F. Nicot. 2014. "Real-scale investigation of the kinematic responses of a rockfall protection embankment." *Nat. Hazard. Earth Syst. Sci.* 14 (5): 1269–1281. https://doi.org/10.5194/nhess-14-1269-2014.

LS-DYNA. 2012. *LS-DYNA keyword user's manual, version 971*. Livermore, CA: Livermore Software Technology.

Muthuswamy, M., and A. Tordesillas. 2006. "How do interparticle contact friction, packing density and degree of polydispersity affect force propagation in particulate assemblies?" *J. Stat. Mech: Theory Exp.* 2006 (9): P09003. https://doi.org/10.1088/1742-5468/2006/09/P09003.

Ng, C. W. W., C. E. Choi, A. Y. Su, J. S. H. Kwan, and C. Lam. 2016. "Large-scale successive impacts on a rigid barrier shielded by gabions." *Can. Geotech. J.* 53 (10): 1688–1699. https://doi.org/10.1139/cgj-2016-0073.

Peila, D., C. Oggeri, and C. Castiglia. 2007. "Ground reinforced embankments for rockfall protection, design and evaluation of full scale tests." *Landslides* 4 (3): 255–265. https://doi.org/10.1007/s10346-007-0081-4.

Schellenberg, K., A. Volkwein, A. Roth, and T. Vogel. 2006. "Rockfall-falling weight tests on galleries with special cushion layers." In *Proc., 3rd Int. Conf. on Protection of Structures against Hazards*, 1–8. Singapore: CI-Premier Conference Organisation.

Schellenberg, K., A. Volkwein, A. Roth, and T. Vogel. 2007. "Large-scale impact tests on rock fall galleries." In *Proc., 7th Int. Conf. on Shock and Impact Loads on Structures*, 497–504. Singapore: CI-Premier Conference Organisation.

Zegowitz, A. 2010. "Cellular glass aggregate serving as thermal insulation and a drainage layer." In Vol. 2010 of *Proc., Buildings Conf.*, 1–8. Atlanta, GA: ASHRAE.

Zeng, C., P. Cui, Z. Su, Y. Lei, and R. Chen. 2015. "Failure modes of reinforced concrete columns of buildings under debris flow impact." *Landslides* 12 (3): 561–571. https://doi.org/10.1007/s10346-014-0490-0.

Zhang, L., N. G. H. Nguyen, S. Lambert, F. Nicot, F. Prunier, and I. Djeran-Maigre. 2017. "The role of force chains in granular materials: From statics to dynamics." *Eur. J. Environ. Civ. Eng.* 21 (7–8): 874–895. https://doi.org/10.1080/19648189.2016.1194332.

Zhao, Y. P. 1998. "Predictions of structural dynamic plastic shear failure by Johnson's damage number." *Forsch. Ingenieurwes.* 63 (11–12): 349–352. https://doi.org/10.1007/PL00010753.